EUROPEAN JOURNAL OF COMPUTATIONAL MECHANICS, 2016
VOL. 25, NO. 3, 273–293
http://dx.doi.org/10.1080/17797179.2016.1191122

Taylor & Francis
Taylor & Francis Group

Comparison of point foot, collisional and smooth rolling contact models on the bifurcations and stability of bipedal walking

W. G. Charles, P. Mahmoodi, R. S. Ransing, I. Sazonov and M. I. Friswell

College of Engineering, Swansea University, Swansea, UK

ABSTRACT

Traditional biped walkers based on passive dynamic walking usually have flat or circular feet. This foot contact may be modelled with an effective rocker – represented as a roll-over shape – to describe the function of the knee–ankle–foot complex in human ambulation. Mahmoodi et al. has represented this roll-over shape as a polygon with a discretised set of collisions. In this paper point foot, collisional and smooth rolling contact models are compared. An approach based on the Lagrangian mechanics is used to formulate the equations for the swing phase that conserves mechanical energy. Qualitative insight can be gained by studying the bifurcation diagrams of gait descriptors such as average velocity, step period, mechanical energy and inter-leg angle for different gain and length values for the feet, as well as different mass and length ratios. The results from the three approaches are compared and discussed. In the case of a rolling disk, the collisional contact model gives a negligible energy loss; incorporated into the double inverted pendulum system, however, reveals much greater errors. This research is not only useful for understanding the stability of bipedal walking, but also for the design of rehabilitative devices such as prosthetic feet and orthoses.

ARTICLE HISTORY
Received 4 October 2015
Accepted 4 May 2016

KEYWORDS
Passive walking; gait analysis; roll-over shape; prosthetic foot; foot contact; bifurcation diagrams; basin of attraction

1. Introduction

An unpowered mechanical biped walker can traverse down an inclined plane with a steady, symmetric gait comparable to human walking (McGeer, 1990). The amount of energy lost at heel strike is made up by the potential energy gained from walking down the slope. These 'compass-like' passive dynamic walkers are usually preferred because of their simplicity and may be used as a tool to analyse efficient bipedal locomotion. Research into the simple point foot model is still being used today, not only as a simple approach to the biomechanics of walking but also for in-depth analysis of the inverted double pendulum dynamics (Chyou et al., 2011; Garcia et al., 1998; Goswami, Thuilot, & Espiau, 1996; Li & Yang, 2012). Other walkers are commonly modelled with flat (Goswami, 1999) or

CONTACT R. S. Ransing r.s.ransing@swansea.ac.uk

curved/circular feet; however it has been shown that foot kinematics has a direct influence on the stability of a bipedal robot (Mahmoodi, Ransing, & Friswell, 2013). This rolling contact may be modelled using an effective rocker to describe the function of the knee–ankle–foot complex in human walking as shown in Figure 1. This effective rocker can be obtained from the physiological roll-over shape defined as the trajectory of the centre of pressure in the local co-ordinate system aligned with the stance leg (Miff et al., 2008). A roll-over shape can be determined experimentally from motion capture systems and ground reaction measurement. The roll-over shape represents the knee–ankle–foot kinematics, whereas the majority of bipedal walking models would have a single point foot contact at the end of the leg. From numerous studies it has been shown that an individual's roll-over shape does not change appreciably with walking speed (Hansen, Childress, & Knox, 2004), with shoe heel height (Hansen & Childress, 2004) or when carrying extra weight (Hansen & Childress, 2005). Modelling the physiological knee–ankle–foot system can give a better understanding of its functions during able-bodied gait and can improve the stability of designs for ankle-foot prosthesis and orthoses. Using the roll-over function in order to predict the movement of hip mass can reduce the number of degrees of freedom, while still matching kinematics as the flexions of ankles, knees and other muscles or bones are incorporated within the roll-over concept. Basin of attraction plots (Schwab & Wisse, 2001), (Li & Yang, 2012) and bifurcation diagrams (Goswami, Thuilot, & Espiau 1996) are often used to study the stability and periodicity of bipedal walking. This paper compares the effect of using three computational models to capture the hip, ankle, foot kinematics and study its influence on predicting the stability and periodicity of the walking process. In Section 2, it is described how point foot, collisional and smooth rolling foot contact models are used to approximate the hip, ankle and foot kinematics. The roll-over shape concept is introduced and the formulations of the three mathematical models are compared. The conditions used to compare the walking steps (and rolling disc comparison) are described in Section 3 and the results are discussed in Section 4. The paper is concluded in Section 5 with a discussion on future challenges.

2. Incorporating foot contact into a biped walker

2.1. Roll-over function definition

Hip-ankle-foot roll-over shapes are obtained first by attaching markers to the hip and ankle then plotting the trajectory in a global coordinate system as shown in Figure 1(a). The Centre of Pressure (CoP) location is also obtained via ground reaction force plates. A local coordinate system is then defined by aligning the axis along the stance leg as in Figure 1(b). In this way, the knee–ankle–foot system can be simplified into a rigid rocker attached at the end of the leg. The roll-over

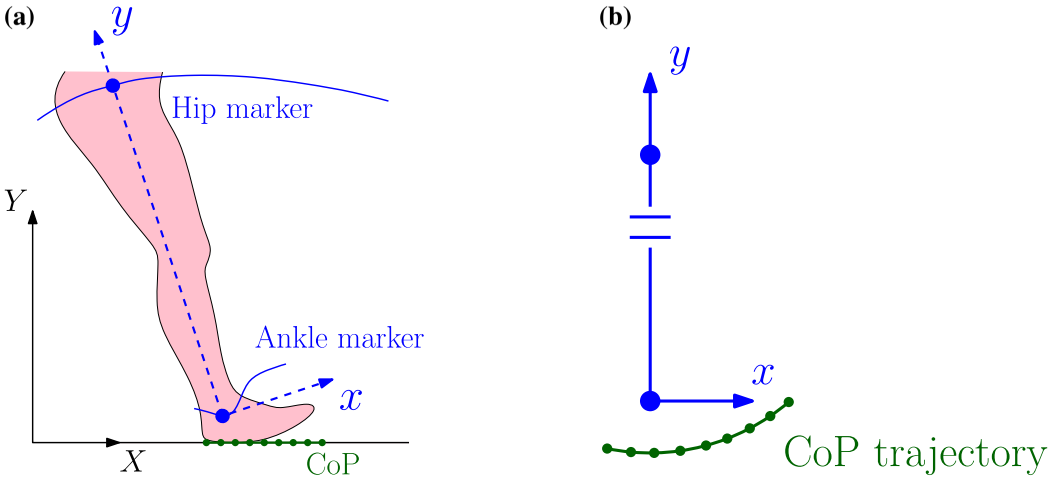

Figure 1. Roll-over shape is obtained from motion capture data and applied to a passive dynamic walker to match the trajectory of the hip mass. (a) Markers show the trajectory of the ankle and hip, while force plates obtain the CoP locations in a laboratory-based coordinate system. (b) Trajectory of Centre of Pressure plotted in a local coordinate system aligned with the stance leg.

function $y = f(x)$ is assumed to be a simple polynomial function

$$f(x) = \frac{1}{r}(x - x_m)^2 + y_m \tag{1}$$

which is comparable to a curve with a constant radius of curvature. r represents the curvature of the foot and will be referred to as the 'roll-over gain'. x_m and y_m represent the coordinates of the x, y frame when the stance leg is vertical ($\theta_1 = 0$). At the end of the roll-over shape, rolling contact is locked and the rocker will act as a pivot point at the end of the foot. In a human system, this can be comparable to rocking on the heel or the metatarsals at the ball of the foot.

2.2. Discretised collisions to emulate the rolling contact

Mahmoodi, Ransing, and Friswell (2013) modelled this rolling contact as a concave polygon as shown in Figure 2(b). In this model, the stance leg pivots about pivot point 1 with inverted pendulum dynamics until pivot point 2 makes contact with the floor. At this point, there is a completely inelastic collision. A transition occurs that conserves the angular momentum of the walker using the initial conditions that consists of virtual leg lengths, initial angular velocities and initial angular displacements. As the number of pivot points across the polygon increase, less energy will be lost during the swing phase. This approach was done in order to overcome the inability to model the complex non-circular geometry of roll-over shapes. Before this, only point contact or curved/circular feet could be used. The details of the equations of motion for the collisional pivot point model are discussed in the following Section 2.3. From this study, an interest was gained in the qualitative analysis using a complex roll-over shape in an inverted pendulum passive dynamic model. A method of still incorporating a roll-over function as the foot contact, without the need for discretising the rolling contact as a set of collisions is proposed in Section 2.4. Both of these methods can easily be simplified into the point foot model.

2.3. Collisional equations to emulate rolling contact (Mahmoodi, Ransing, & Friswell, under review)

The parameters for the collisional rolling walking model can be seen in Figure 1(a). The upper body mass m_H is concentrated at the hip joint, while the leg masses are defined as m_s and m_{ns}. The vector $\boldsymbol{\theta} = [\theta_s, \theta_{ns}]^T$ with θ_s and θ_{ns} being the angles made by, respectively, the support leg and the swinging leg. We define l_{vs} as the virtual stance leg length and a_{vs} as the virtual stance lower leg length, with θ_{vsl} and θ_{vs} being the angles made, respectively. For both models the dynamical equations can be derived from the Euler-Lagrange approach:

$$\frac{\mathrm{d}}{\mathrm{d}t}\left(\frac{\partial \mathcal{L}(\boldsymbol{\theta}, \dot{\boldsymbol{\theta}})}{\partial \dot{\boldsymbol{\theta}}}\right) - \frac{\partial \mathcal{L}(\boldsymbol{\theta}, \dot{\boldsymbol{\theta}})}{\partial \boldsymbol{\theta}} = 0 \tag{2}$$

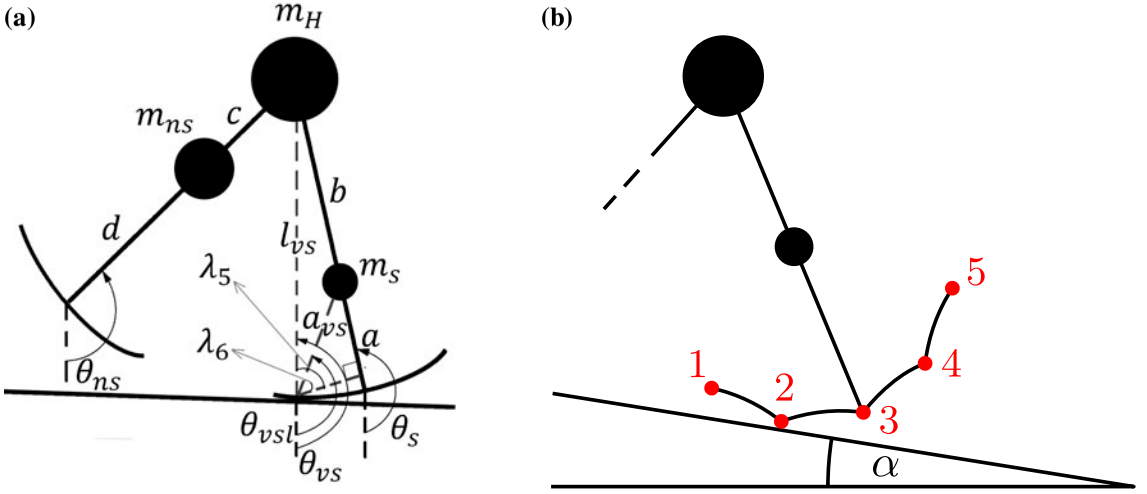

Figure 2. The collisional rolling model described by Mahmoodi, Ransing, and Friswell (2013). The roll-over shape outlined in Equation 1 is discretised into a concave polygon to emulate the rolling contact. (a) Coordinate system for the model proposed by Mahmoodi et al. (b) Rolling collision model with 5 pivot points along a circular arc at an inclined plane with angle α.

where the Lagrangian $\mathcal{L}(\boldsymbol{\theta}, \dot{\boldsymbol{\theta}})$ is the difference between kinetic and potential energies $\mathcal{L}(\boldsymbol{\theta}, \dot{\boldsymbol{\theta}}) = K(\boldsymbol{\theta}, \dot{\boldsymbol{\theta}}) - P(\boldsymbol{\theta})$. For the collisional model, the double pendulum equations of motion as the system rotates around each pivot point, i, is derived in Appendix A.1. These equations can be described as

$$\boldsymbol{M}^i(\boldsymbol{\theta})\ddot{\boldsymbol{\theta}} + \boldsymbol{N}^i(\boldsymbol{\theta}, \dot{\boldsymbol{\theta}})\dot{\boldsymbol{\theta}} + \boldsymbol{g}^i(\boldsymbol{\theta}) = 0 \tag{3}$$

with $\boldsymbol{M}$, $\boldsymbol{N}$ and $\boldsymbol{g}$ defined as

$$\boldsymbol{M}^i(\boldsymbol{\theta}) = \begin{pmatrix} m_s {a^i_{vs}}^2 + m_H {l^i_{vs}}^2 + m_{ns} {l^i_{vs}}^2 & -m_{ns} l^i{}_{vs} c \cos(\theta_{vs} - \theta_{ns}) \\ -m_{ns} l^i{}_{vs} c \cos(\theta_{vs} - \theta_{ns}) & m_{ns} c^2 \end{pmatrix} \tag{4}$$

$$\boldsymbol{N}^i(\boldsymbol{\theta}, \dot{\boldsymbol{\theta}}) = \begin{pmatrix} 0 & -m_{ns} l^i_{vs} c \dot{\theta}_{ns} \sin(\theta_{vs} - \theta_{ns}) \\ m_{ns} l^i_{vs} c \dot{\theta}_{ns} \sin(\theta_{vs} - \theta_{ns}) & 0 \end{pmatrix} \tag{5}$$

$$\boldsymbol{g}^i(\boldsymbol{\theta}) = \begin{pmatrix} m_s g a^i_{vs} \sin\theta_{vsl} + (m_H g l^i_{vs} + m_{ns} g l^i_{vs}) \sin(\theta_{vs}) \\ -mgc \sin(\theta_{ns}) \end{pmatrix} \tag{6}$$

and the superscript i referring to the ith pivot point. What makes the collisional model unique is the idea that the rolling contact is modelled with a large number of discrete collisions. If the next pivot point, $i + 1$ comes into contact with the ground a completely inelastic collision occurs, at which point pivot point i will leave the ground. The following instantaneous collision takes place:

$$\dot{\boldsymbol{\theta}}^{i+} = \frac{\boldsymbol{H}^i(\boldsymbol{\theta})}{\boldsymbol{H}^i_d} \dot{\boldsymbol{\theta}}^{i-} \tag{7}$$

where the superscripts $^-$ and $^+$ indicate, respectively, pre-impact and post-impact variables. This equation represents the conservation of angular momentum at each inelastic collision during the swing phase and the terms for $\boldsymbol{H}^i$ are given by

$$\begin{aligned} H^i_{11} = {} & m_H l^i_{vs} l^{i-1}_{vs} c \cos(\theta^+_{vs} - \theta^-_{vs}) + m_s a^i_{vs} a^{i-1}_{vs} c \cos(\theta^+_{vsl} - \theta^-_{vsl}) \\ & + m_{ns} l^i_{vs} l^{i-1}_{vs} c \cos(\theta^+_{vs} - \theta^-_{vs}) - m_{ns} l^i_{vs} l^{i-1}_{vs} c \cos(\theta^-_{vs} - \theta_{ns}) \cos(\theta^+_{vs} - \theta_{ns}) \end{aligned} \tag{8}$$

$$H^i_{12} = 0 \tag{9}$$

$$\begin{aligned} H^i_{21} = {} & \left(m_H + m_{ns}\right) {l^i_{vs}}^2 l^{i-1}_{vs} \cos(\theta^+_{vs} - \theta_{ns}) \cos(\theta^+_{vs} - \theta^-_{vs}) \\ & + m_s l^i_{vs} a^i_{vs} a^{i-1}_{vs} \cos(\theta^+_{vs} - \theta_{ns}) \cos(\theta^+_{vsl} - \theta^-_{vsl}) \\ & - \left(m_H + m_{ns}\right) {l^i_{vs}}^2 l^{i-1}_{vs} \cos(\theta^-_{vs} - \theta_{ns}) - m_s l^{i-1}_{vs} {a^i_{vs}}^2 \cos(\theta^-_{vs} - \theta_{ns}) \end{aligned} \tag{10}$$

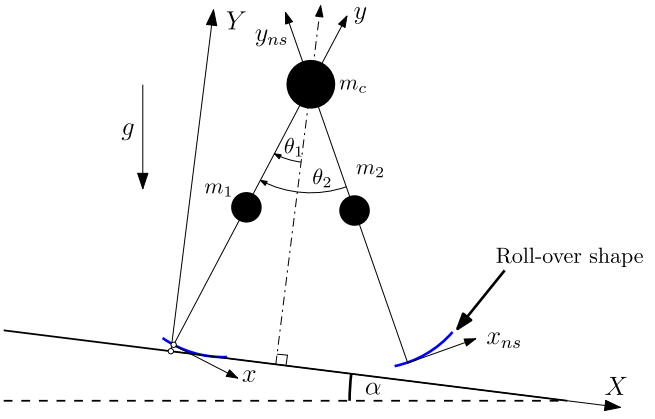

Figure 3. Smooth rolling contact model with a hip mass and a point mass at each leg. The roll-over shape from Equation 1 is included at the end of each leg.

$$H^i_{22} = H^i_d = m_H {l^i_{vs}}^2 c + m_s {a^i_{vs}}^2 c + m_{ns} {l^i_{vs}}^2 c - m_{ns} {l^i_{vs}}^2 c \cos^2(\theta^{i+}_{vs} - \theta^{i+}_{ns}) \quad (11)$$

Note that $H^i_{21} \rightarrow 0$ as the number of pivot points increase. Equations 7–11 are needed for the single-support phase exclusively for the collisional model. These equations are used to model the contact as a set of collisions during this phase, unlike in the rolling contact model, where the contact is modelled smoothly by the roll-over function.

2.4. Smooth rolling contact model

The new biped model is shown in Figure 3. The model's configuration can be described by $\boldsymbol{\theta} = [\theta_1, \theta_2]^T$ with θ_1 being the angle made between the support leg with the normal to the ground and θ_2 the angle between the support leg and the non-support swinging leg. Note that this reference frame is slightly different to the one proposed in Section 2.3. The state vector $\boldsymbol{q}$ associated with the robot is then:

$$\boldsymbol{q} = [\boldsymbol{\theta}, \dot{\boldsymbol{\theta}}]^T = [\theta_1, \theta_2, \dot{\theta}_1, \dot{\theta}_2]^T \quad (12)$$

The motion of the stance leg is determined by the roll-over shape having form $y = f(x)$ Equation 1 in the reference frame defined $\{x, y\}$ above. The analogous reference frame $\{x^{ns}, y^{ns}\}$ describes the non-support swinging leg. Values for the

inertia matrix from Equation 3 are now given by:

$$\boldsymbol{M}(\boldsymbol{\theta}) = \begin{pmatrix} \Theta_1 & \Theta_{12} \\ \Theta_{12} & \Theta_2 \end{pmatrix} \tag{13}$$

$$\boldsymbol{N}(\boldsymbol{\theta}, \dot{\boldsymbol{\theta}}) = \begin{pmatrix} \frac{1}{2}\frac{\partial \Theta_1}{\partial \theta_1}\dot{\theta}_1 + \frac{1}{2}\frac{\partial \Theta_1}{\partial \theta_2}\dot{\theta}_2 & \frac{1}{2}\frac{\partial \Theta_1}{\partial \theta_2}\dot{\theta}_1 + \left(\frac{1}{2}\frac{\partial \Theta_2}{\partial \theta_1} - \frac{\partial \Theta_{12}}{\partial \theta_2}\right)\dot{\theta}_2 \\ \left(\frac{1}{2}\frac{\partial \Theta_1}{\partial \theta_2} - \frac{\partial \Theta_{12}}{\partial \theta_1}\right)\dot{\theta}_1 + \frac{1}{2}\frac{\partial \Theta_2}{\partial \theta_1}\dot{\theta}_2 & \frac{1}{2}\frac{\partial \Theta_2}{\partial \theta_1}\dot{\theta}_1 + \frac{1}{2}\frac{\partial \Theta_2}{\partial \theta_2}\dot{\theta}_2 \end{pmatrix} \tag{14}$$

$$\boldsymbol{g}^T(\boldsymbol{\theta}) = \begin{pmatrix} \frac{\partial P}{\partial \theta_1} & \frac{\partial P}{\partial \theta_2} \end{pmatrix} \tag{15}$$

with Θ_1, Θ_{12} and Θ_2 are given by:

$$\Theta_1 = m_1\left(\left(\frac{\partial X_1}{\partial \theta_1}\right)^2 + \left(\frac{\partial Y_1}{\partial \theta_1}\right)^2\right) + m_c\left(\left(\frac{\partial X_c}{\partial \theta_1}\right)^2 + \left(\frac{\partial Y_c}{\partial \theta_1}\right)^2\right) \tag{16}$$

$$+m_2\left(\left(\frac{\partial X_2}{\partial \theta_1}\right)^2 + \left(\frac{\partial Y_2}{\partial \theta_1}\right)^2\right) \tag{17}$$

$$\Theta_{12} = m_2\left(\frac{\partial X_2}{\partial \theta_1}\frac{\partial X_2}{\partial \theta_2} + \frac{\partial Y_2}{\partial \theta_1}\frac{\partial Y_2}{\partial \theta_2}\right) \tag{18}$$

$$\Theta_2 = m_2\left(\left(\frac{\partial X_2}{\partial \theta_2}\right)^2 + \left(\frac{\partial Y_2}{\partial \theta_2}\right)^2\right) \tag{19}$$

P being the potential energy given in the appendix Equation (B3) and the coordinates for each point mass $[X_1, Y_1]$, $[X_2, Y_2]$ & $[X_c, Y_c]$ in Equations (B4)-(B10).

2.5. The double support transition phase

The walkers have rigid, non-elastic legs so there is assumed to be a completely non-elastic collision at heel strike. The contact made with the floor with the swinging leg results in an instantaneous impact with no slipping. Point foot, collisional and the smooth-rolling models have the same inelastic collision at each step. As the body configuration remains unchanged during impact, the change in angular positions is represented by the equation

$$\boldsymbol{\theta}^+ = \boldsymbol{J}\boldsymbol{\theta}^- \tag{20}$$

where the superscripts $^-$ and $^+$ indicate, respectively, pre-impact and post-impact variables and the matrix $\boldsymbol{J}$ for the collisional and smooth-rolling models is found in Appendices A.2 and B.2, respectively. Conservation of angular momentum leads to the condition:

$$\dot{\boldsymbol{\theta}}^+ = \frac{\boldsymbol{Q}^-(\theta)}{\boldsymbol{Q}^+(\theta)}\dot{\boldsymbol{\theta}}^- \tag{21}$$

with the matrixes for $\boldsymbol{Q}^-$ and $\boldsymbol{Q}^+$ for the collisional and smooth rolling models are given in Appendices A.2 and B.2, respectively. The point model uses the same mathematics as the rolling contact; however, the hindfoot and forefoot lengths are set to 0. This means that with no foot contact the walker rotates around a pivot point at the 'ankle'.

3. Results

3.1. Rolling disk verification for the collisional model

The drawbacks of discretising the rolling contact is that this approach is unable to conserve mechanical energy through the infinitesimal jumps that occur as the walker rolls over from one pivot point to another throughout the swing phase. However, with a large number of points on a curve, the mechanical losses can be negligible, represented with the case of a ball rolling down a slope as shown in Figure 4. A circular disk is represented as a concave polygon with a large number of corners or pivot-points and set to roll down a slope, where NP is the number of pivot points. The analytical equation for acceleration is $g \sin(\alpha)$, with α being the angle of slope. An average walking step takes around 0.6–0.7s, while the rolling disk solution gives good results up to 4 sec with NP=7962. Equation 3 is solved using MATLAB's in-built Runge-Kutta numerical integration method 'ode45'. The approach described in Section 2.4 is computationally more efficient and provides more accurate results by conserving mechanical energy throughout the swing phase. Hence, it will give a greater insight into the dynamics of bipedal locomotion.

3.2. Comparing one walking step

The parameters for the model can be non-dimensionalised in order to reduce the number of free parameters. A mass ratio is defined as the ratio of hip mass, m_H to leg mass, m, while a length ratio is the ratio of upper leg length, b, to lower leg length, a (refer to Figure 2(a)). Roll-over gain is defined in Equation 1 and represents curvature of the foot. Physiological values for the three point masses can be used by inspecting body dimensions and centre of mass locations for the legs. The Naval Biodynamics Laboratory (1988) yield a mass and length ratio of 3.5822 and 0.6, respectively. The walking incline is set to 2° to give a good steady walking speed for all models. The foot contact for the discrete and smooth rolling contact models have a roll-over gain, r, of 1.2 as in Equation 1. The hindfoot length is 6.2 cm and forefoot length 17.8 cm. The collisional model has 3400 points distributed along the foot. By using exactly the same model parameters and initial conditions, we can evaluate the results at the evolution of one walking step. Values are converted from the coordinate system defined in Figure 3 into coordinates as in Figure 2(a) in order to compare the two models. The smooth rolling contact is completely conservative during the swing phase, while the collisional contact has a difference in energy of 0.14% as shown in

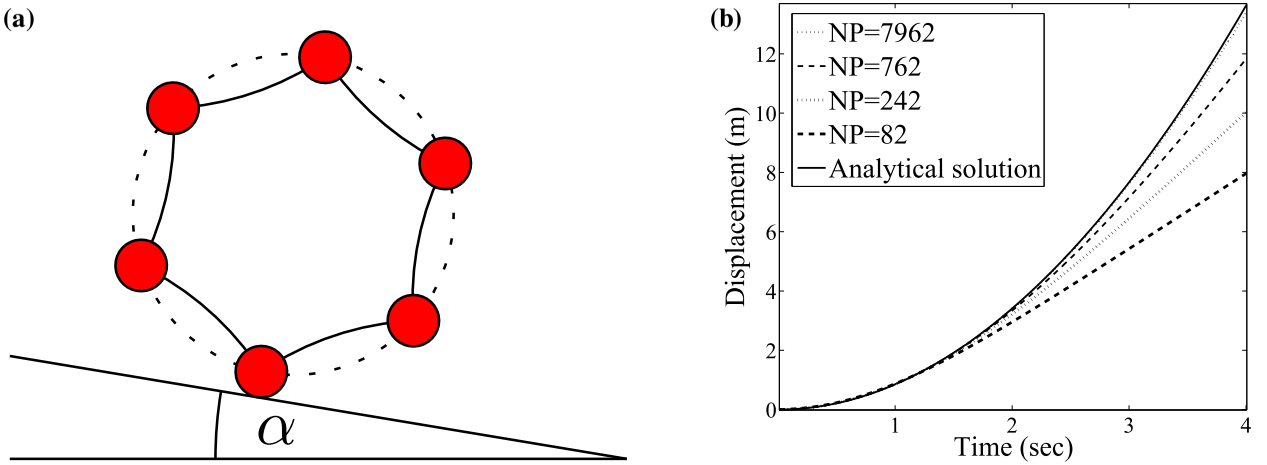

Figure 4. Rolling disk is discretised into NP points with a completely inelastic transfer collision occurring at each pivot point. (a) Circular disk represented as a concave polygon with NP corners. Each corner is said to be a 'pivot point' for the collisional model. (b) Results for the collisional contact model for a rolling disk on an inclined surface of 4°.

Figure 5(a). Figure 5(b) proves that loss of this energy is related to the length of the foot. Figure 6 shows the difference in angular displacements and velocities, $\boldsymbol{\theta}$ and $\dot{\boldsymbol{\theta}}$. Although the rolling disk in Section 3.1 showed negligible divergence at 0.7 sec, there appears to be some divergence during rolling contact in a walking model. The swing leg diverges, while the stance leg seems to remain. As this system is a double inverted pendulum, it is likely that the swing leg mass is sensitive to even the slightest perturbation.

3.3. Bifurcation diagrams

Bifurcation diagrams can be used to show gait factors such as inter-leg angle, step period and average velocity as a function of model parameters. The walker is set in motion for 40 steps, at which point it is assumed to be stable and values for the next 10 steps are plotted. Bifurcation diagrams show certain behaviour such as periodic asymmetric walking that leads to chaotic behaviour. Parameters of a robot walker can include slope angle, mass ratios and leg length ratios, while different curvatures for the feet can also be compared to see how this affects the dynamics of human locomotion. The bifurcation diagrams outlined in Figure 7 show the evolution of step period and inter-leg angle as a function of slope angle. The model parameters are the same as in Section 3.2. From the following figures, it can be seen that the collisional model enters the chaotic region at shallower inclines. In a passive biped walker, the slope angle is increased in order to increase the potential energy at each walking step to offset the energy lost at heel strike. With the multiple collisional model, an increased amount of energy is lost during the swing phase as the model rolls along the foot contact. This is different to the point foot and smooth rolling models in which mechanical energy is completely conserved during the swing phase.

3.4. Basin of Attraction

At heel strike, there are three initial conditions that can have an effect on the stability of the walker; angle between the legs, θ_2 and the angular velocities of both legs, $\dot{\theta}_1$ & $\dot{\theta}_2$. Studying the basin of attraction will give us a good indication of the stability of a walker (Schwab & Wisse, 2001). The walker is set to walk with a set of initial conditions up to 50 steps. If the walker manages to reach 50 steps, the walker is said to be stable and that set of initial conditions lies inside the basin of attraction. Figure 8 shows the boundaries of basin of attraction comparison to show the robustness of the walker at a range of initial conditions. In simple terms, a greater area of basin of attraction shows that the walker will be less likely to fall over due to perturbations. As the computation time of the smooth rolling contact model is approximately 60 times faster than the collision model, the speed of calculation for the basin of attraction can be greatly increased.

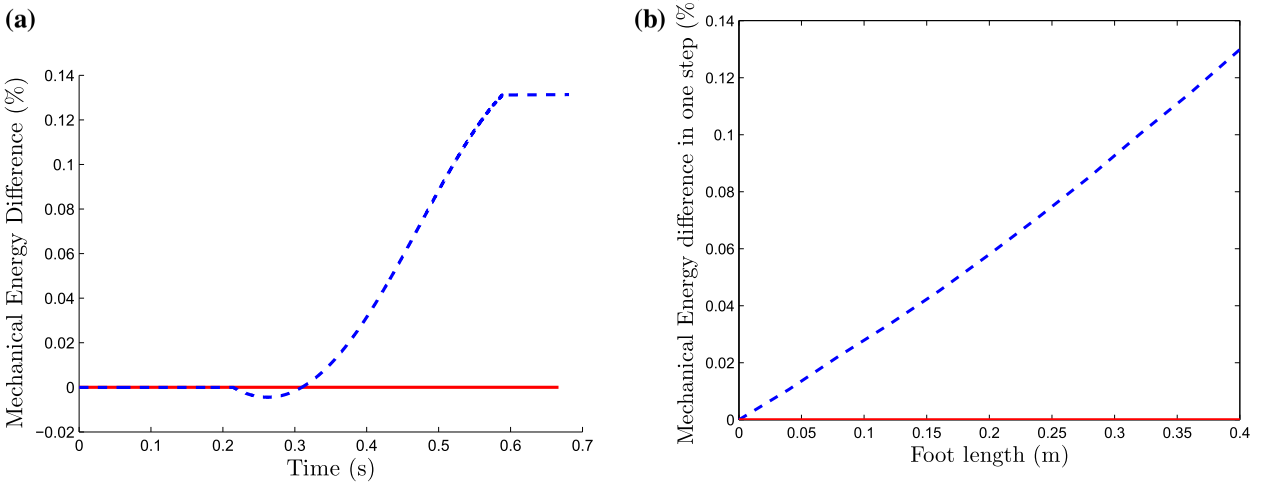

Figure 5. Mechanical Energy difference with the collisional and rolling contact models. The blue line shows the mechanical energy difference in the collisional model, while the red line shows that the analytical solution has constant mechanical energy throughout the stance phase. (a) Mechanical energy difference in stance phase time with physiological values. Hindfoot length of 0.062 m and a forefoot length of 0.178 m. Mechanical Energy at the initial start is 698.23 J. (b) Mechanical losses from the collisional model at a fixed number of discrete pivot points with increasing foot lengths. Foot has a gain of 1.2 and is symmetric at the ankle joint.

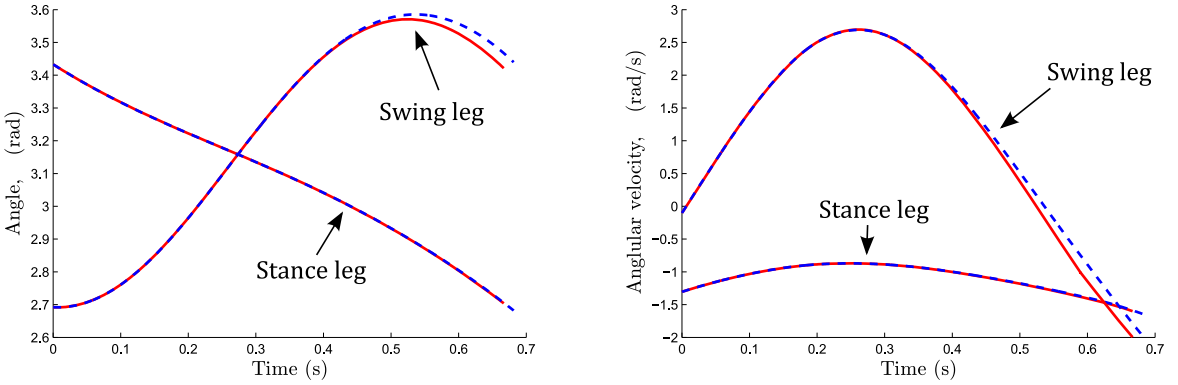

Figure 6. Angular displacement and velocity variation at one walking step with the same initial conditions. The blue dotted line is the collision model, red is rolling contact model.

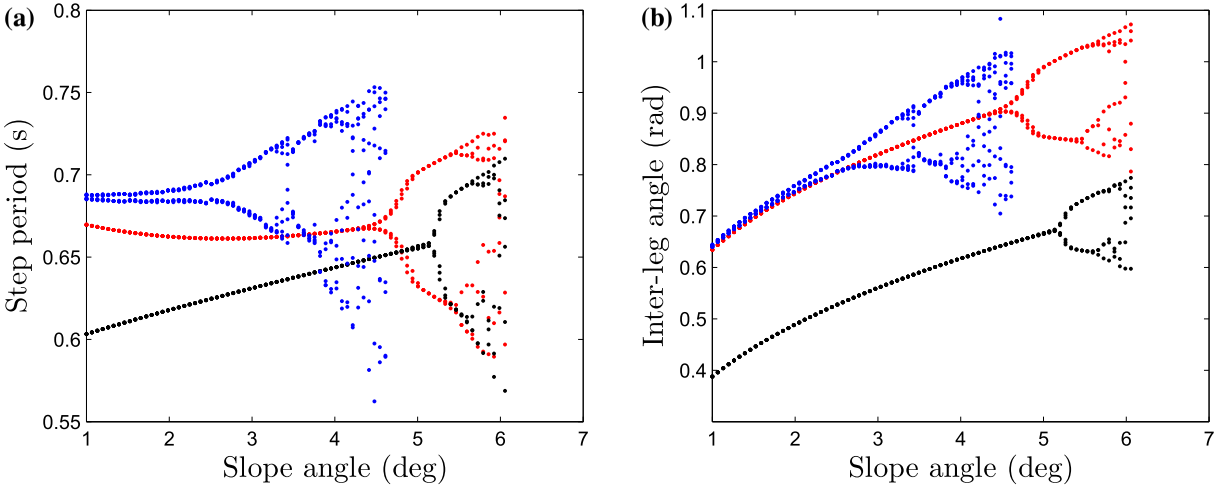

Figure 7. Bifurcation diagrams for inter-leg angle and step period for stable walking at steps 40-50. The black dots are for the point foot model, the blue represents collisional rolling and red shows the smooth rolling contact model. (a) Step period bifurcation diagram evaluates the time taken at each step. (b) inter-leg angle between the two legs at heel strike.

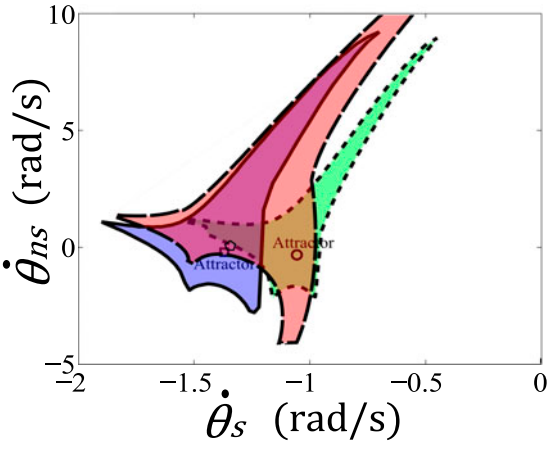

Figure 8. Basin of Attraction for the pivot point (green, dotted), rolling collision (blue, normal line) and smooth rolling (red, dashed) contact models.

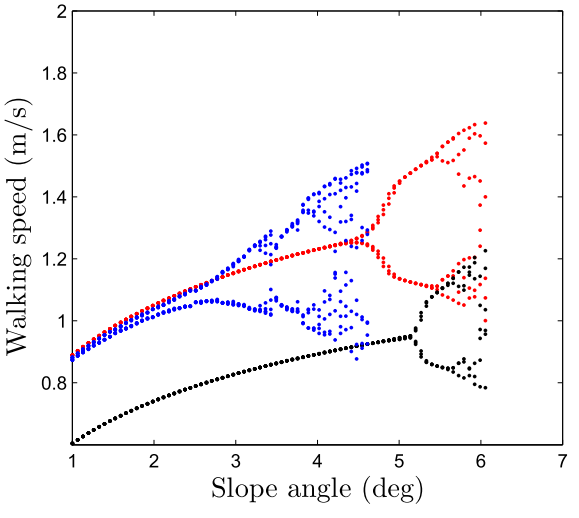

Figure 9. Average walking speed at a given slope angle for the point foot model (black) and with physiological foot contact (red).

4. Discussion of results

The point foot model is usually used as a simplification for bipedal walking; however, there can be seen to be a large difference in gait descriptors at a given slope angle. Using a roll-over shape can give better walking speed without going into the chaotic region Figure 9. A physiological walking speed is said to be around 1.4 m/s. Although with a roll-over gain, r, of 1.2 the average velocity is 1.25 m/s before bifurcating, for passive walking this is a great improvement from 0.95 m/s for the point foot model. Differences between the collisional and smooth rolling models are due to the error in mechanical energy at the collisions of each

pivot point in the swing phase. Although the difference should be negligible as in the rolling disk benchmark in Section 3.1, the actual deviation is noticeable. It should be noted that the double inverted pendulum mechanics is a chaotic system, so a small deviation from one walking step could possibly lead to a greater difference at stable walking or up to a convergence at around 20–50 walking steps. An important aspect of the mechanical system is the point at which bifurcation occurs. In further work, it will be interesting to compare both models until the transition to a chaotic region. The basin of attraction plots (Figure 8) show the robustness of using smooth rolling contact over the point foot or the collisional model. The smooth rolling contact model has maximum overlapping area with the other two models. However, the basin of attraction area is different for each model. This reinforces the importance of the hypothesis that the smooth rolling contact should be preferred over collisional and point foot models. Before the bifurcation region both models are comparable, however computationally the smooth rolling model is approximately 60 times faster. This substantial increase in speed is particularly advantageous when performing basin of attraction work, in which computational times are demanding.

5. Conclusions

The point foot single mass model is usually preferred for its simplicity. However, we believe it is worth adapting the point model to include rolling contact in order to make the results more accurate without needing to increase the number of DoF. The rolling contact gives a better estimation for the trajectory of CoM and hence can more accurately predict the dynamics of human walking. Using rolling contact also increases the stability (Figure 8) and average walking velocity for a given slope angle (Figure 9). Using multiple collisions to simulate rolling contact seemed to yield accurate results with a very large number of pivot points on a rolling disk; however, incorporated into the double pendulum mechanics it makes a much larger difference with the swing leg. This leads to differences on the time of heel-strike, in addition to step length and touch-down velocity. An analytical approach for modelling a rolling contact in a biped walker with a roll-over shape has been presented and compared with collisional rolling and point foot model. This approach conserves mechanical energy throughout the stance phase and can be used to more accurately predict gait descriptors such as average velocity, step period, mechanical energy and inter-leg angle for different gain and length values for the feet, as well as different mass and length ratios. This is particularly useful when incorporating roll-over shapes obtained experiments of the human system. This study has shown insight into the fact that even a negligible deviation in mechanical energy can have a great effect on the double inverted pendulum dynamics. Future passive walking systems should consider using the roll-over shape to more accurately predict the trajectory of hip mass without increasing the number of DoF in a system. The next task is to compare

results with unbalanced mass distributions in order to explore prosthetic design applications such as the work by Mahmoodi, Ransing, and Friswell (under review). Future work can also include adding a linear or torsional spring in order to emulate the muscle contractions in human walking and compare the ground reaction forces with experimental data (Geyer, Seyfarth, & Blickhan, 2006; Kuo, Donelan, & Ruina, 2005). This research is not only useful in order to improve stability and correct gait for the design of prosthetic feet, but also for rehabilitative devices such as ankle-foot orthoses (Mahmoodi, Ransing, & Friswell, under review; Richter et al., 2015).

Disclosure statement

No potential conflict of interest was reported by the authors.

Funding

The authors gratefully acknowledge the financial support provided by the Sêr Cymru National Research Network in Advanced Engineering and Materials [grant number NRN019].

ORCID

R. S. Ransing http://orcid.org/0000-0003-4848-4545

References

Chyou, T., Liddell, G. F., & Paulin, M. G. (2011). An upper-body can improve the stability and efficiency of passive dynamic walking. *Journal of Theoretical Biology, 285*, 126–135.

Hansen, A. H., & Childress, D. S. (2004). Effects of shoe heel height on biologic rollover characteristics during walking. *Journal of Rehabilitation Research and Development, 41*, 547–554.

Hansen, A. H., & Childress, D. S. (2005). Effects of adding weight to the torso on roll-over characteristics of walking. *Journal of Rehabilitation Research and Development, 42*, 381–390.

Hansen, A. H., Childress, D. S., & Knox, E. H. (2004). Roll-over shapes of human locomotor systems: Effects of walking speed. *Clinical Biomechanics (Bristol, Avon), 19*, 407–414.

Garcia, M., Chatterjee, A., Ruina, A., & Coleman, M. (1998). The simplest walking model: Stability, complexity, and scaling. *Journal of Biomechanical Engineering*, *120*, 281–288.

Geyer, H., Seyfarth, A., & Blickhan, R. (2006). Compliant leg behaviour explains basic dynamics of walking and running. *Proceedings of the Royal Society B: Biological Sciences, 273*, 2861–2867.

Goswami, A. (1999). Postural stability of biped robots and the foot-rotation indicator (FRI) Point. *The International Journal of Robotics Research, 18*, 523–533.

Goswami, A., Thuilot, B., & Espiau, B. (1996). Compass-like biped robot Part I : Stability and bifurcation of passive gaits. [Research Report] RR-2996, INRIA.

Kuo, A. D., Donelan, J. M., & Ruina, A. (2005). Energetic consequences of walking like an inverted pendulum: Sstep-to-step transitions. *Exercise and Sport Sciences Reviews, 33*, 88–97.

Li, Q., & Yang, X. S. (2012). New walking dynamics in the simplest passive bipedal walking model. *Applied Mathematical Modelling, 36*, 5262–5271.

Mahmoodi, P., Ransing, R. S., & Friswell, M. I. (2013). Modelling the effect of heel to toe roll-over contact on the walking dynamics of passive biped robots. *Applied Mathematical Modelling, 37*, 7352–7373.

Mahmoodi, P., Ransing, R. S., & Friswell, M. I. (2016). A novel mathematical formulation for predicting symmetric passive bipedal walking motion with unbalanced masses. *Applied Mathematical Modelling, 40*, 3895–3906. doi:10.1016/j.apm.2015.10.051

McGeer, T. (1990). Passive dynamic walking. *The International Journal of Robotics Research, 9*, 62–82.

Miff, S. C., Hansen, A. H., Childress, D. S., Gard, S. A., & Meier, M. R. (2008). Roll-over shapes of the able-bodied knee–ankle–foot system during gait initiation, steady-state walking, and gait termination. *Gait & Posture, 27*, 316–322.

Naval Biodynamics Laboratory (1988). *Anthropometry and mass distribution for human analogues*. Report Number NBDL-87R003. Bethesda, MD: Naval Medical Research and Development Office.

Richter, H., Simon, D., Smith, W. A., & Samorezov, S. (2015). Dynamic modeling, parameter estimation and control of a leg prosthesis test robot. *Applied Mathematical Modelling, 39*, 559–573.

Schwab, A. L., & Wisse, M. (2001). Basin of attraction of the simplest walking model. *Proceedings of the ASME Design Engineering Technical Conference, 6*, 531–539.

Appendix 1. Collisional rolling model mechanics

A.1. Derivation of Equation 3 ($M^i(\theta)\ddot{\theta} + N^i(\theta,\dot{\theta})\dot{\theta} + g^i(\theta) = 0$) using the Euler-Langrangian approach for the single support phase

The Euler-Lagrange equation for each pivot point of the concave polygon, i

$$\frac{\mathrm{d}}{\mathrm{d}t}\left(\frac{\partial L^i(\theta,\dot{\theta})}{\partial\dot{\theta}}\right) - \frac{\partial L^i(\theta,\dot{\theta})}{\partial\theta} = 0, \qquad L^i(\theta,\dot{\theta}) = K^i(\theta,\dot{\theta}) - P^i(\theta) \tag{A1}$$

Kinetic energy $K^i(\theta,\dot{\theta})$ and potential energy $P^i(\theta)$ are given by:

$$K^i(\theta,\dot{\theta}) = \frac{1}{2}m_H\|\vec{v}_H\|^2 + \frac{1}{2}m_s\|\vec{v}_s\|^2 + \frac{1}{2}m_{ns}\|\vec{v}_{ns}\|^2 \tag{A2}$$

$$P^i(\theta) = -m_H g l^i_{vs}\cos\theta_{vs} - m_s g a^i_{vs}\cos\theta_{vsl} - m_{ns}g\left(l^i_{vs}\cos\theta_{vs} - c\cos\theta_{ns}\right) \tag{A3}$$

and the velocities of each point mass are given by

$$\begin{aligned}\overrightarrow{v_H} &= l_{vs}\dot{\theta}_s\cos\theta_{vs}\vec{i} + l_{vs}\dot{\theta}_s\sin\theta_{vs}\vec{j}\\ \overrightarrow{v}_s &= a_{vs}\dot{\theta}_s\cos\theta_{vsl}\vec{i} + a_{vs}\dot{\theta}_s\sin\theta_{vsl}\vec{j}\\ \overrightarrow{v_{ns}} &= \left(l_{vs}\dot{\theta}_s\cos\theta_{vs} - c\dot{\theta}_{ns}\cos\theta_{ns}\right)\vec{i} + \left(l_{vs}\dot{\theta}_s\sin\theta_{vs} - c\dot{\theta}_{ns}\sin\theta_{ns}\right)\vec{j}\end{aligned} \tag{A4}$$

A.2. The double-support phase momentum transfer

An instantaneous impact for the double support transition occurs in all models. The double support phase for the collisional model has been derived from Mahmoodi, Ransing, & Friswell (under review) and is as follows: The matrix $\boldsymbol{J}$ in Equation (20) takes the form

$$\boldsymbol{J} = \begin{bmatrix}0 & 1\\ 1 & 0\end{bmatrix} \tag{A5}$$

At double-support, due to the conservation of angular momentum, the following equation relates the pre-impact and post-impact angular velocities:

$$\dot{\boldsymbol{\theta}}^{1+} = \frac{\boldsymbol{Q}^{-}(\boldsymbol{\theta})}{\boldsymbol{Q}^{+}} \dot{\boldsymbol{\theta}}^{1-} \tag{A6}$$

where elements of $\boldsymbol{Q}^{-}(\boldsymbol{\theta})$

$$\begin{aligned}
Q_{11}^{-} &= m_H m_s b^2 l_{vs}^{e-} l_{vs}^{1+} \cos(\theta_{vs}^{-} - \theta_{vs}^{+}) + m_s^2 b^2 l_{vs}^{1+} a_{vs}^{e-} \cos(\theta_{vs}^{+} - \theta_{vsl}^{-}) \\
&\quad + m_s m_{ns} b^2 l_{vs}^{e-} a_{vs}^{1+} \cos(\theta_{vsl}^{+} - \theta_{vs}^{-}) \\
&\quad - m_s^2 b^2 l_{vs}^{1+} a_{vs}^{e-} \cos(\theta_{ns}^{+} - \theta_{vsl}^{-}) \cos(\theta_{vs}^{+} - \theta_{ns}^{+}) \\
Q_{12}^{-} &= -m_s m_{ns} b^2 c a_{vs}^{1+} \cos(\theta_{vsl}^{+} - \theta_{ns}^{-}) \qquad \text{(A7)} \\
Q_{21}^{-} &= m_s m_H b l_{vs}^{e-} l_{vs}^{1+2} \cos(\theta_{vs}^{+} - \theta_{ns}^{+}) \cos(\theta_{vs}^{-} - \theta_{vs}^{+}) \\
&\quad + m_s^2 b a_{vs}^{e-} l_{vs}^{1+2} \cos(\theta_{vs}^{+} - \theta_{ns}^{+}) \cos(\theta_{vs}^{+} - \theta_{vsl}^{-}) \\
&\quad + m_s m_{ns} b l_{vs}^{e-} l_{vs}^{1+} a_{vs}^{1+} \cos(\theta_{vs}^{+} - \theta_{ns}^{+}) \cos(\theta_{vsl}^{+} - \theta_{vs}^{-}) \qquad \text{(A8)} \\
&\quad - m_s m_H b a_{vs}^{e-} l_{vs}^{1+2} \cos(\theta_{ns}^{+} - \theta_{vsl}^{-}) \\
&\quad - m_s m_{ns} b a_{vs}^{e-} a_{vs}^{1+2} \cos(\theta_{ns}^{+} - \theta_{vsl}^{-}) - m_s^2 b a_{vs}^{e-} l_{vs}^{1+2} \cos(\theta_{ns}^{+} - \theta_{vsl}^{-}) \\
Q_{22}^{-} &= -m_s m_{ns} b c l_{vs}^{1+} a_{vs}^{1+} \cos(\theta_{vsl}^{+} - \theta_{ns}^{-}) \cos(\theta_{vs}^{+} - \theta_{ns}^{+}) \qquad \text{(A9)} \\
Q^{+} &= m_s b^2 (m_H l_{vs}^{1+2} + m_s l_{vs}^{1+2} + m_{ns} a_{vs}^{1+2} - m_s l_{vs}^{1+2} \cos^2(\theta_{vs}^{+} - \theta_{ns}^{+})) \qquad \text{(A10)}
\end{aligned}$$

and e represents the eth pivot point.

Appendix 2. Mathematical derivation of smooth rolling contact method outlined in Section 2.4.

B.1. Swing phase mechanics

The planar double-pendulum equations are adapted to include roll-over support for the foot contact. Its dynamical equations are derived from the Euler-Lagrange approach:

$$\frac{\mathrm{d}}{\mathrm{d}t}\left(\frac{\partial \mathcal{L}(\boldsymbol{\theta}, \dot{\boldsymbol{\theta}})}{\partial \dot{\boldsymbol{\theta}}}\right) - \frac{\partial \mathcal{L}(\boldsymbol{\theta}, \dot{\boldsymbol{\theta}})}{\partial \boldsymbol{\theta}} = 0 \tag{B1}$$

where the Lagrangian $\mathcal{L}(\boldsymbol{\theta}, \dot{\boldsymbol{\theta}})$ is the difference between kinetic and potential energies $\mathcal{L}(\boldsymbol{\theta}, \dot{\boldsymbol{\theta}}) = K(\boldsymbol{\theta}, \dot{\boldsymbol{\theta}}) - P(\boldsymbol{\theta}, \dot{\boldsymbol{\theta}})$.

$$K(\boldsymbol{\theta}, \dot{\boldsymbol{\theta}}) = \frac{1}{2} m_H \|\vec{\boldsymbol{v}}_H\|^2 + \frac{1}{2} m_s \|\vec{\boldsymbol{v}}_s\|^2 + \frac{1}{2} m_{ns} \|\vec{\boldsymbol{v}}_{ns}\|^2 \tag{B2}$$

If the ground plane is at an angle, α, with the horizontal plane ($\alpha < 0$ if walking downhill as in Figure 2b) then the potential energy can be written as

$$P(\boldsymbol{\theta}) = m_H g(X_H \sin\alpha + Y_H \cos\alpha) + m_s g(X_s \sin\alpha + Y_s \cos\alpha) + m_{ns} g(X_{ns} \sin\alpha + Y_{ns} \cos\alpha) \tag{B3}$$

Let point mass m_1 be located in point $\mathbf{P}_1$ having fixed co-ordinates $[x_1, y_1]$ in the $\{x, y\}$ reference frame and point mass m_2 be located in point $\mathbf{P}_2$ having fixed co-ordinates $[x_2^{ns}, y_2^{ns}]$ in the $\{x^{ns}, y^{ns}\}$ reference frame. Also the third mass m_c is located in hip joint at the centre of rotation between $\{x, y\}$ and $\{x^{ns}, y^{ns}\}$ reference frames and having the same co-ordinates, $\{x_c, y_c\}$ in the both frames.

The vectors are given by:

$$\vec{\boldsymbol{v}}_H = \dot{X}_H\vec{\imath} + \dot{Y}_H\vec{\jmath} \tag{B4}$$
$$\vec{\boldsymbol{v}}_s = \dot{X}_s\vec{\imath} + \dot{Y}_s\vec{\jmath} \tag{B5}$$
$$\vec{\boldsymbol{v}}_{ns} = \dot{X}_{ns}\vec{\imath} + \dot{Y}_{ns}\vec{\jmath} \tag{B6}$$

with the coordinates,

$$\begin{aligned} X_1(\theta_1) &= (x_1 - x_\theta(\theta_1))\cos\theta_1 + (y_1 - y_\theta(\theta_1))\sin(\theta_1) + s(\theta_1) \\ Y_1(\theta_1) &= -(x_1 - x_\theta(\theta_1))\sin\theta_1 + (y_1 - y_\theta(\theta_1))\cos(\theta_1) \end{aligned} \tag{B7}$$

$$\begin{aligned} X_c(\theta_1) &= (x_c - x_\theta(\theta_1))\cos\theta_1 + (y_c - y_\theta(\theta_1))\sin(\theta_1) + s(\theta_1) \\ Y_c(\theta_1) &= -(x_c - x_\theta(\theta_1))\sin\theta_1 + (y_c - y_\theta(\theta_1))\cos(\theta_1) \end{aligned} \tag{B8}$$

where functions $x_\theta(\theta_1)$ and $y_\theta(\theta_1)$,

$$\begin{aligned} x_\theta(\theta_1) &= \frac{r\tan(\theta_1)}{2} + x_m \\ y_\theta(\theta_1) &= \frac{r}{4\tan^2(\theta_1)} + y_m \end{aligned} \tag{B9}$$

are defined by rearranging Equation (1). Also for the swinging leg,

$$\begin{aligned} X_2(\theta_1,\theta_2) &= (x_2(\theta_2) - x_\theta(\theta_1))\cos\theta_1 + (y_2(\theta_2) - y_\theta(\theta_1))\sin\theta_1 + s(\theta_1) \\ Y_2(\theta_1,\theta_2) &= -(x_2(\theta_2) - x_\theta(\theta_1))\sin\theta_1 + (y_2(\theta_2) - y_\theta(\theta_1))\cos\theta_1 \end{aligned} \tag{B10}$$

where $[x_2, y_2]$ are coordinates of point $\mathbf{P}_2$ in the $\{x, y\}$ reference frame:

$$\begin{aligned} x_2(\theta_2) &= (x_2^{ns} - x_c)\cos\theta_2 + (y_2^{ns} - y_c)\sin\theta_2 + x_c \\ y_2(\theta_2) &= -(x_2^{ns} - x_c)\sin\theta_2 + (y_2^{ns} - y_c)\cos\theta_2 + y_c \end{aligned} \tag{B11}$$

Inserting Equations B4, B5 and B6 into B2, $K(\boldsymbol{\theta}, \dot{\boldsymbol{\theta}})$ can be rewritten as:

$$K(\boldsymbol{\theta}, \dot{\boldsymbol{\theta}}) = \frac{1}{2}\dot{\boldsymbol{\theta}}^T\boldsymbol{M}(\boldsymbol{\theta})\dot{\boldsymbol{\theta}} \tag{B12}$$

which is comparable to the well-known double pendulum equations with the following form:

$$\boldsymbol{M}(\boldsymbol{\theta})\ddot{\boldsymbol{\theta}} + \boldsymbol{N}(\boldsymbol{\theta}, \dot{\boldsymbol{\theta}})\dot{\boldsymbol{\theta}} + \boldsymbol{g}(\boldsymbol{\theta}) = 0 \tag{B13}$$

B.2. Double-support phase for the smooth contact model

Section 2.5 outlines the double support phase: At post impact the leading becomes the swinging leg and the trailing leg becomes the stance leg. This leads to the equation

$$\boldsymbol{J} = \begin{bmatrix} 1 & 1 \\ 0 & -1 \end{bmatrix} \tag{B14}$$

and

$$\mathbf{Q}^-\dot{\boldsymbol{\theta}}^- = \mathbf{Q}^+\dot{\boldsymbol{\theta}}^+ \tag{B15}$$

where the matrix $\mathbf{Q}^{-}$ consists of

$$\begin{aligned} Q_{11}^{-} = m_H & \left(\frac{\partial Y_H}{\partial \theta_1^-}(X_H^+ - s^+) - \frac{\partial X_H}{\partial \theta_1^-} Y_H \right) \\ & + m_1 \left(\frac{\partial Y_1}{\partial \theta_1^-}(X_1^+ - s^+)) - \frac{\partial X_1}{\partial \theta_1^-} Y_1 \right) \\ & + m_2 \left(\frac{\partial Y_2}{\partial \theta_1^-}(X_2^+ - s^+) - \frac{\partial X_2}{\partial \theta_1^-} Y_2 \right) \end{aligned} \tag{B16}$$

$$Q_{12}^{-} = m_2 \left(\frac{\partial Y_2}{\partial \theta_2^-}(X_H^+ - s^+) - \frac{\partial X_2}{\partial \theta_2^-} Y_2 \right) \tag{B17}$$

$$Q_{21}^{-} = m_1 \left(\vec{X_c X}_{1pre} \frac{\partial Y_1}{\partial \theta_1^-} - \vec{Y_c Y}_{1pre} \frac{\partial X_1}{\partial \theta_1^-} \right) \tag{B18}$$

$$Q_{22}^{-} = 0 \tag{B19}$$

and the matrix for post-impact, $\mathbf{Q}^{+}$:

$$\begin{aligned} Q_{11}^{+} = m_H & \left(\frac{\partial Y_H^+}{\partial \theta_1^+}(X_H^+ - s^+) - \frac{\partial X_H^+}{\partial \theta_1^+} Y_H^+ \right) \\ & + m_1 \left(\frac{\partial Y_1^+}{\partial \theta_1^+}(X_1^+ - s^+) - \frac{\partial X_1^+}{\partial \theta_1^+} Y_1 \right) \\ & + m_2 \left(\frac{\partial Y_2}{\partial \theta_1^+}(X_2^+ - s^+) - \frac{\partial X_2}{\partial \theta_1^+} Y_c \right) \end{aligned} \tag{B20}$$

$$Q_{12}^{+} = m_1 \left(\frac{\partial Y_2}{\partial \theta_2^+}(X_2^+ - s^+) - \frac{\partial X_2}{\partial \theta_2^+} Y_2 \right) \tag{B21}$$

$$Q_{21}^{+} = m_1 \left(\vec{X_c X}_{1post} \frac{\partial Y_2}{\partial \theta_1^+} - \vec{Y_c Y}_{1post} \frac{\partial X_2}{\partial \theta_1^+} \right) \tag{B22}$$

$$Q_{22}^{+} = m_1 \left(\vec{X_c X}_{1post} \frac{\partial Y_2}{\partial \theta_2^+} - \vec{Y_c Y}_{1post} \frac{\partial X_2}{\partial \theta_2^+} \right) \tag{B23}$$